Human Molecular Genetics, 2015, Vol. 24, No. 3 637–648
doi:10.1093/hmg/ddu477
Advance Access published on September 16, 2014

Dominant mutations in ORAI1 cause tubular aggregate myopathy with hypocalcemia via constitutive activation of store-operated Ca^{21} channels

Yukari Endo[1,2,4], Satoru Noguchi[1,2,*], Yuji Hara[5,6], Yukiko K. Hayashi[1,2,7], Kazushi Motomura[1], Satoko Miyatake[8], Nobuyuki Murakami[9], Satsuki Tanaka[10], Sumimasa Yamashita[11], Rika Kizu[12], Masahiro Bamba[13], Yu-ichi Goto[1,3], Naomichi Matsumoto[8], Ikuya Nonaka[2] and Ichizo Nishino[1,2]

[1]Department of Clinical Development, Translational Medical Center, National Center of Neurology and Psychiatry, Kodaira, Tokyo 187-8556, Japan, [2]Department of Neuromuscular Research and [3]Department of Mental Retardation and Birth Defect Research, National Institute of Neuroscience, National Center of Neurology and Psychiatry, Kodaira, Tokyo 187-8502, Japan, [4]Department of Pediatrics, Kyoto University Graduate School of Medicine, Kyoto 606-8507, Japan, [5]Department of Synthetic Chemistry and Biological Chemistry, Graduate School of Engineering, Kyoto University, Kyoto 615-8510, Japan, [6]Tokyo Women's Medical University Institute for Integrated Medical Sciences (TIIMS), Shinjuku, Tokyo 162-8666, Japan, [7]Department of Neurophysiology, Tokyo Medical University, Tokyo 160-8402, Japan, [8]Department of Human Genetics, Graduate School of Medicine, Yokohama City University, Yokohama 236-0004, Japan, [9]Department of Pediatrics, Dokkyo Medical University, Koshigaya Hospital, Koshigaya, Saitama 343-8555, Japan, [10]Department of Diabetes and Endocrinology, Osaka Saiseikai Nakatsu Hospital, Osaka 530-0012, Japan, [11]Division of Pediatric Neurology, Kanagawa Children's Medical Center (KCMC), Yokohama 232-8555, Japan, [12]Division of Pediatrics, Yokosuka Kyosai Hospital, Yokosuka, Kanagawa 238-8558, Japan and [13]Division of Pediatrics, Kawasaki Municipal Hospital, Kawasaki, Kanagawa 210-0013, Japan

Received June 28, 2014; Revised August 26, 2014; Accepted September 10, 2014

The store-operated Ca^{21} release-activated Ca^{21} (CRAC) channel is activated by diminished luminal Ca^{21} levels in the endoplasmic reticulum and sarcoplasmic reticulum (SR), and constitutes one of the major Ca^{21} entry pathways in various tissues. Tubular aggregates (TAs) are abnormal structures in the skeletal muscle, and although their mechanism of formation has not been clarified, altered Ca^{21} homeostasis related to a disordered SR is suggested to be one of the main contributing factors. TA myopathy is a hereditary muscle disorder that is pathologically characterized by the presence of TAs. Recently, dominant mutations in the STIM1 gene, encoding a Ca^{21} sensor that controls CRAC channels, have been identified to cause tubular aggregate myopathy (TAM). Here, we identified heterozygous missense mutations in the ORAI1 gene, encoding the CRAC channel itself, in three families affected by dominantly inherited TAM with hypocalcemia. Skeletal myotubes from an affected individual and HEK293 cells expressing mutated ORAI1 proteins displayed spontaneous extracellular Ca^{21} entry into cells without diminishment of luminal Ca^{21} or the association with STIM1. Our results indicate that STIM1-independent activation of CRAC channels induced by dominant mutations in ORAI1 cause altered Ca^{21} homeostasis, resulting in TAM with hypocalcemia.

*To whom correspondence should be addressed at: Department of Neuromuscular Research, National Institute of Neuroscience, National Center of Neurology and Psychiatry, 4-1-1, Ogawahigashi-cho, Kodaira, Tokyo 187-8502, Japan. Tel: +81 423461712; Fax: +81 423461742. Email: noguchi@ncnp.go.jp

INTRODUCTION

Calcium (Ca^{2+}) signals are crucial for controlling a broad range of cellular functions, including secretion, excitation, contraction, motility, metabolism, transcription, growth, cell division and apoptosis (1). In the striated muscle, the sarcoplasmic reticulum (SR) is a primary Ca^{2+}-storage organelle, and Ca^{2+} released from the SR directly activates the contraction of myofibrils via excitation – contraction coupling regulation (2). Depletion of Ca^{2+} in the SR activates a store-operated Ca^{2+} entry (SOCE) pathway that is used to replenish intracellular calcium stores (3,4). In non-excitable cells and the skeletal muscle, SOCE is coordinated by stromal-interacting molecule 1 (STIM1), an endoplasmic reticulum (ER)/SR Ca^{2+} sensor, and ORAI1, a plasma membranous calcium release-activated Ca^{2+} (CRAC) channel, following Ca^{2+} ion release from intracellular stores (5 – 8). Specifically, when the ER/SR Ca^{2+} store is depleted, oligomerization and translocation of STIM1 to adjacent ER/SR-plasma membrane junctions are induced (9). Within these junctions, oligomeric STIM1 interacts with and activates ORAI1 (10–12).

Recessive mutations in ORAI1 are known to cause severe combined immunodeficiency (SCID, MIM 612782), which is characterized by a severe defect in T-cell activation accompanied by muscle hypotonia (13,14). In this disease, mutated ORAI1 leads to its deficiency in the plasma membrane resulting in loss of function of SOCE. Homozygous nonsense mutations in STIM1 also cause primary immunodeficiency (15) (MIM612783). Recently, dominant missense mutations in STIM1 were revealed to cause tubular aggregate myopathy (TAM) (16). TAM is a rare form of myopathy that can show either autosomal-dominant or -recessive inheritance (17), and is pathologically characterized by the presence of tubular aggregates (TAs). A gain of function of mutated STIM1 due to disruption of its Ca^{2+}-sensing domain was suggested as the main pathomechanism underlying STIM1-related TAM. More recently, Stormorken syndrome, which is characterized by thrombocytopenia, muscle fatigue, asplenia and congenital miosis, was also reported to be caused by a gain-of-function STIM1 mutation (18,19). Stormorken syndrome displays histological evidence of myopathy with TAs (18). However, the mechanism underlying muscle weakness and TA formation from abnormal Ca^{2+} influx has not been well established.

TAs are abnormal structures in muscle fibers that are morphologically characterized based on light and electron microscopic observations (20,21). TAs appear as accumulations of densely packed tubules, which are suggested to arise from the SR as they contain numerous SR proteins (21,22). Conceivably, the formation of TAs is triggered by some functional consequences due to disruptions in the SR-T-tubule junction, such as altered Ca^{2+} homeostasis (20). Alternatively, TAs are thought to be derived from reshaping of the SR caused by aggregation of misfolded membranous proteins (23). TAs are also observed in certain types of muscle diseases, including periodic paralysis, congenital myasthenic syndromes, alcohol- and drug-induced myopathy and TAM (21,22). However, the precise mechanism of TA formation remains to be clarified.

In this study, we performed whole exome sequencing in three families suffering from genetically undiagnosed TAM and found pathogenic mutations in the ORAI1. In addition, we demonstrated STIM1-independent activation of CRAC channels in myotubes derived from an affected individual, suggesting that this abnormal activation is the basic mechanism of this disease.

RESULTS

Clinical characterization of individuals with TAM

The clinical features of the included families are listed in Table 1 and Supplementary Material, Table S1. The common characteristic symptoms among the families were diffuse muscle weakness, marked and bilateral ankle joint contractures, rigid spine and hypocalcemia. Disease onset ranged from childhood to adolescence. Muscle weakness progressed slowly, and although all of the affected individuals were ambulant, half of them required the use of high-heeled shoes to walk correctly. All affected members in Family A and Family B showed mildly decreased serum Ca^{2+} levels and relatively low intact parathyroid hormone (PTH) levels, which were still within the normal range. In computed tomography imaging of II-3a, III-2a and II-3b, paraspinal, gastrocnemius and soleus muscles were markedly replaced by fat, which might explain ankle joint contractures and rigid spine. Trapezius, latissimus dorsi, gluteus medius, hamstrings and adductor muscles in the thigh showed severe atrophy and fat infiltration (Fig. 1). Affected members in Family A also showed central nervous system involvement as follows: individual II-3a showed calcification in the cerebellum, basal ganglia and cerebral corticomedullary junction; individual III-2a showed mild intellectual disability (IQ: 63, based on the Weschler Intelligence Scale for Children III). None of the included individuals showed characteristic signs of Stormorken syndrome, such as congenital miosis, bleeding diathesis and thrombocytopenia (Supplementary Material, Table S1).

Pathological findings

TAs were found in muscle fibers of four affected individuals (II-3a in Fig. 2; I-2b and II-1c in Supplementary Material, Fig. S1; II-1b, pictures not shown). The TAs appeared as bright red inclusions in muscle fibers following modified Gomori trichrome (mGt) staining (Fig. 2A) and showed high enzymatic activity following NADH-tetrazolium reductase (NADH-TR) staining (Fig. 2B), but were negative for succinate dehydrogenase (SDH) expression (Fig. 2C), reflecting characteristics of the SR but not the mitochondria. Under electron microscopy, the TAs appeared as aggregates composed of numerous straight tubules aligned in parallel in a longitudinal dimension and were arranged in a honeycomb-like structure in the transverse dimension (Fig. 2D). At higher magnification, each tubule showed double-walled membranes (Fig. 2E and F). All these findings were compatible with previously reported features of TAs (20). In addition to TAs, all biopsy samples demonstrated chronic dystrophic changes based on the presence of regenerating fibers, increased internal nuclei, fiber size variation in both type 1 and type 2 fibers and endomysial fibrosis. Type 1 fiber predominance was also observed (Table 2).

The ORAI1 gene is mutated in TAM-affected individuals

In order to identify the genetic cause of dominantly inherited TAM, we performed whole exome sequencing on two affected

Table 1. Clinical characterization of TAM families

	Family A		Family B			Family C
	II-3	III-2	I-2	II-1	II-3	II-1
Sex	Female	Male	Female	Female	Male	Male
Mutation	c.292G.A	c.292G.A	c.292G.A	c.292G.A	c.292G.A	c.412C.T
Predicted protein impact	p.Gly98Ser	p.Gly98Ser	p.Gly98Ser	p.Gly98Ser	p.Gly98Ser	p.Leu138Phe
Muscle disorders						
Onset	Childhood	Childhood	NI	Childhood	Childhood	Adolescence
Patterns of weakness	Lower limbs proximal; upper limbs proximal	Diffuse	Diffuse	Diffuse	Diffuse	Diffuse
Disease course	Slowly progressive	Slowly progressive	Slowly progressive	Slowly progressive	Slowly progressive	Slowly progressive
Serum CK (IU/L) (normal range)	65 (45–170)	1300 (61–255)	300 (–200)	960 (–200)	684 (–200)	213 (37–142)
Joint contractures						
Onset	Childhood	Childhood	NI	Childhood	Childhood	Adolescence
Ankle	Bilateral, severe	Bilateral, severe	Bilateral, severe	Bilateral, severe	Bilateral, severe	NI
Surgical treatment	NP	NP	13 years old	10 years old	11 years old	NP
Rigid spine	+	+	+	+	+	+
Hypocalcemia						
Onset	Childhood	Childhood	NI	Childhood	Neonatal	NI
Serum calcium (mg/dl) (normal range)	7.7 (8.8–10.2)	8.5 (8.8–10.2)	8.1 (9.0–10.2)	7.7 (9.0–10.2)	7.8 (9.0–10.2)	NI
Serum intact PTH (pg/ml) (normal range)	9 (10–65)	NI (NI)	26 (10–65)	22 (10–65)	19 (10–65)	NI
Treatment	+	+	NI	NI	+	
Other symptoms	Diabetes, calcification in the brain	Intellectual disability	–	–	–	–

NI, no information; NP, not performed; CK, creatinine kinase.

(II-3a and III-2a) and two non-affected members (I-2a and III-2a) of Family A and in all five members of Family B (I-1b, I-2b, II-1b, II-2b and II-3b) (Fig. 3A and Supplementary Material, Table S2). In total, 41 variants from Family A and 34 variants from Family B were extracted based on the assumption of autosomal-dominant inheritance and with reference to the dbSNP135, the 1000 Genomes Project database, the National Heart, Lung, and Blood Institute (NHLBI) Exome Variant Server and Human Genetic Variation Database (HGVD) for Japanese genetic variants (Supplementary Material, Table S3). Among all extracted variants, we identified only one common variant, a heterozygous c.292G.A mutation in ORAI1 (RefSeq accession number NM_032790.3) in both families (Table 1 and Fig. 3A and Supplementary Material, Tables S4 and S5). This mutation was confirmed by Sanger sequencing in all affected members and was absent in the unaffected members (Supplementary Material, Fig. S2). We also found an additional heterozygous missense mutation, c.412C.T in ORAI1, in the third TAM family by Sanger sequencing (Fig. 3A and Supplementary Material, Fig. S2). The mutation was not listed in dbSNP137, 1000 Genomes or HGVD. Both mutations were predicted to result in amino acid changes in the ORAI1 protein: p.Gly98Ser in the transmembrane (TM) 1 domain and p.Leu138Phe in the TM2 domain (Fig. 3B). The amino acid residues Gly at 98 and Leu at 138 show high evolutionary conservation (Fig. 3C). The impact of these variations was also predicted to be damaging based on in silico analysis with SIFT and PolyPhen-2 (data not shown). The crystal structure of Drosophila Orai1 determined by Hou et al. (24) and reported in the Molecular Modeling Database (MMDB ID: 105660) (Fig. 3D) shows that Gly98 is localized to face to the pore of the CRAC channel (white) and Leu138 is in the interface between TM1 and 2 (yellow).

Localization and expression of ORAI1 in the skeletal muscles from TAM

To analyze the localization of ORAI1 in the skeletal muscles of TAM, we investigated skeletal muscle cryosections from an individual with TAM (II-3a, II-1c) using immunohistochemistry (Fig. 4). SERCA1, an SR protein, was strongly labeled in the aggregates, as previously reported (20,21). ORAI1 and STIM1 co-localized with SERCA1 in the aggregates. Moreover, dihydropyridine receptor (DHPR), which is present in T-tubules, was also involved in the aggregates and co-localized with ORAI1, as expected (21) (Fig. 4).

On western blotting, the expression levels of ORAI1, STIM1, SERCA1 and SERCA2 in the skeletal muscles from an affected individual (II-1c) were similar to that of the skeletal muscles from unaffected individuals (Supplementary Material, Fig. S3).

TAM cells showed constitutive extracellular Ca^{21} influx via the CRAC channel without depletion of SR Ca^{21} stores

To explore whether the identified mutations are pathogenic, we monitored Ca^{2+} entry into myotubes prepared from muscle cells of an affected individual with the c.292G.A (p.Gly98Ser) mutation. Intracellular Ca^{2+} concentration ($[Ca^{2+}]_i$) was monitored using Fura-2 as a Ca^{2+} indicator and was recorded by using fluorescence ratiometry with excitation at 340 and 380 nm. The experiments revealed a significantly higher $[Ca^{2+}]_i$ level in TAM myotubes than in control cells [normal human skeletal

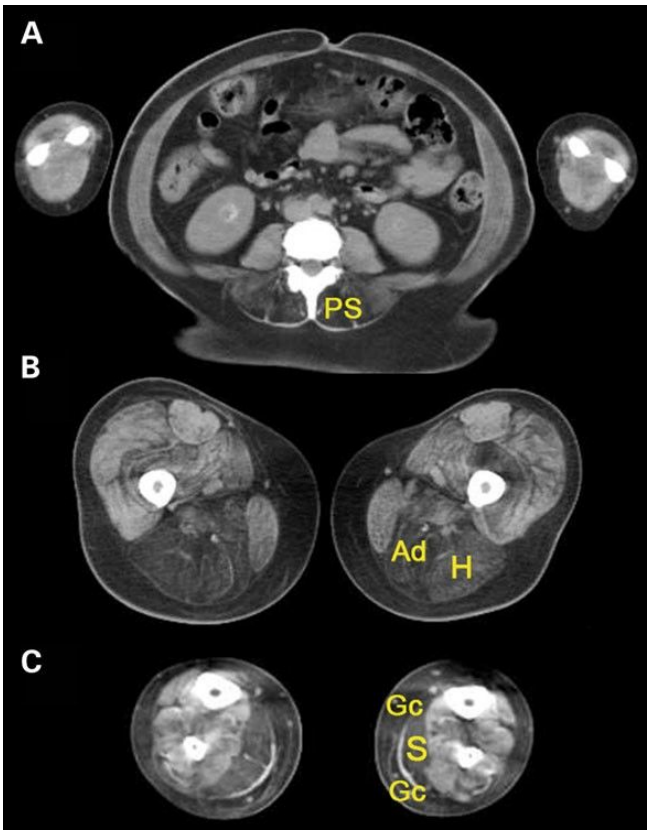

Figure 1. Computed tomographic imaging of TAM. Paraspinal (PS), hamstrings (H), adductor muscles in the thigh (Ad), soleus (S) and gastrocnemius (Gc) muscles of affected individual II-3a were markedly replaced by fat.

muscle cells (SKMCs)] when the extracellular Ca^{2+} concentration was 2 mM, which was assumed to match that of the in vivo environment, and 20 mM (Fig. 5A and B). Upon application of a CRAC channel inhibitor, 50 mM 2-aminoethoxydiphenyl borate [2-APB (25)] or 10 mM 3,5-bistrifluoromethyl pyrazole derivative (BTP2) (26), the $[Ca^{2+}]_i$ levels in TAM myotubes were not elevated (Fig. 5A). Another inhibitor, 1-[2-(4-methoxyphenyl)-2-[3-(4-methoxyphenyl) ethyl-1H-imidazole hydrochloride (SKF-96365), was also effective although the response was slower. These results indicated that the higher Ca^{2+} influx in TAM myotubes occurred via CRAC channels. In addition, an Mn^{2+} quenching assay of intracellular Fura-2 fluorescence was performed (Fig. 5C). Mn^{2+} is known to enter cells via CRAC channels and shows very high affinity to Fura-2. The extracellular Mn^{2+} influx causes quenching of intracellular Fura-2 fluorescence. TAM myotubes showed an Mn^{2+} quenching that was distinct from that of normal myotubes, implicating the activation of CRAC channels. We also examined thapsigargin (TG) treatment to TAM myotubes to induce Ca^{2+} depletion in the SR. TG induced extracellular Ca^{2+} influx in normal myotubes in a dose-dependent manner in extracellular 2 mM Ca^{2+} medium. On the other hand, similar extracellular Ca^{2+} influx levels were observed in TAM myotubes with and without TG treatment (Fig. 5D). Thus, TAM cells showed constitutive Ca^{2+} influx to the cytosol via the CRAC channel without depletion of the SR Ca^{2+} store. It should be noted that slightly higher $[Ca^{2+}]_i$ elevation was observed with higher concentrations of TG treatment (Fig. 5D), indicating that the store-operated Ca^{2+} influx-inducing system may still function in TAM myotubes.

Gly98Ser and Leu138Phe mutations in ORAI1 caused spontaneous activation of the CRAC channel

We also tested the impact of the c.292G.A (Gly98Ser) and c.412C.T (Leu138Phe) mutations in ORAI1 on induction of spontaneous Ca^{2+} influx. $[Ca^{2+}]_i$ was measured at 24–36 h after transfection to HEK293 cells of mutated and wild-type ORAI1 cDNAs. The transfected green fluorescent protein (GFP)-tagged ORAI1 and Myc-tagged ORAI1 localized on the plasma membranes, and the mutated ORAI1 also localized to the cell surface membrane (Fig. 6A). Western blotting of expressed ORAI1 protein showed multiple bands at 25–50 kDa, indicating the presence of different glycosylated forms, similar to previous reports (27,28) (Fig. 6B). Although glycosylated forms of Gly98Ser-mutated ORAI1 were slightly decreased, there were no differences in band patterns observed among Gly98Ser-mutated, Leu138Phe-mutated and wild-type (WT) ORAI1 after PNGase F treatment.

The Gly98Ser and Leu138Phe ORAI1 mutants caused a dramatic elevation of $[Ca^{2+}]_i$ following application of 2 mM Ca^{2+} in the medium when compared with the WT protein (2 mM Ca^{2+} in Fig. 6C). Cells transfected with the Gly98Ser or Leu138Phe mutants exhibited high levels of $[Ca^{2+}]_i$ even under conditions of extracellular Ca^{2+} depletion (0 mM Ca^{2+} region in Fig. 6C). In addition, the Mn^{2+} quenching assay revealed that the cells transfected with Gly98Ser or Leu138 Phe mutants showed distinct Mn^{2+} quenching rates from those transfected with the WT protein (Fig. 6D). It should be noted that the spontaneous Ca^{2+} and Mn^{2+} influx observed in the mutated ORAI1-expressing cells did not require co-expression of STIM1 or TG-induced Ca^{2+} store depletion in the ER. Moreover, the elevated resting $[Ca^{2+}]_i$ induced by both ORAI1 mutants was reduced by application of 2-APB (Supplementary Material, Fig. S4), which indicated the specific activation of CRAC channels. These results clearly demonstrate that both the c.292G.A (Gly98Ser) and c.412C.T (Leu138Phe) mutations in ORAI1 cause constitutive CRAC channel activation in a STIM1-independent manner.

DISCUSSION

Based on the inheritance mode in the affected families and the functional analyses of mutated ORAI1 proteins, we concluded that the constitutive activation of CRAC channels by dominant mutations in ORAI1 caused TAM in the three families. In support of this notion, dominant mutations in STIM1 have been reported to cause TAM by constitutive activation of SOCE (16). In that report, the mutated STIM1 spontaneously clustered and translocated to the plasma membrane independently of Ca^{2+} stores in the SR, and consequently led to activation of the CRAC channel, resulting in higher cytosolic Ca^{2+} levels. More recently, Nesin et al. (18) reported that activating mutations in STIM1 and ORAI1 caused overlapping syndromes of TAM and congenital miosis. Interestingly, the authors suggested that a dominant mutation in ORAI1 caused prolonged activation

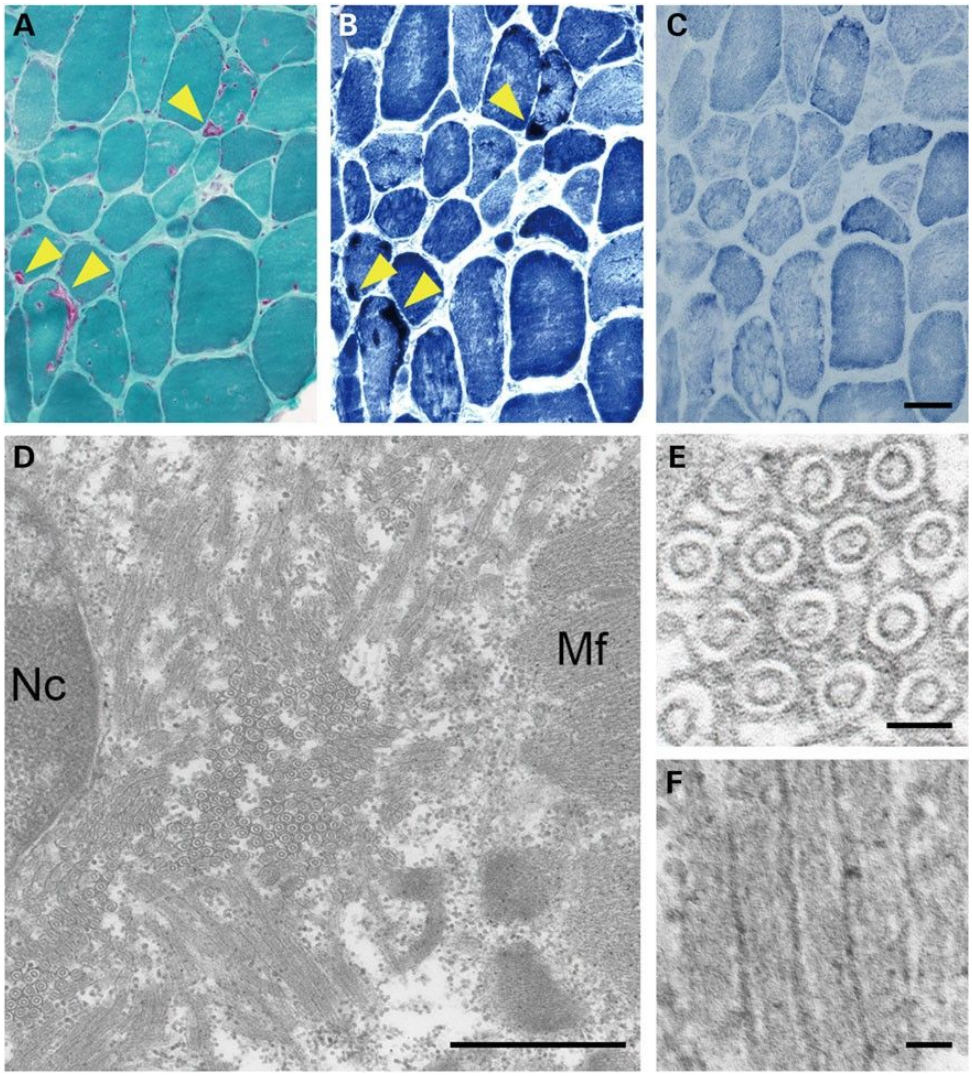

Figure 2. Histology and electron microscopy of a muscle biopsy sample from affected individual II-3a. Histological analysis of transverse sections revealed aggregations with mGt (A) and NADH-TR (B) but not SDH (C) staining. Ultrastructural analysis demonstrated prominent tubular aggregation with double-walled membranes in transversal (D and E) and longitudinal (F) sections. Nc, nucleus; Mf, myofibrils. Arrows, tubular aggregates (TAs). Scale bars, 50 mm (C); 1 mm (D); 100 nm (E); 50 nm (F).

of CRAC channels that required association with STIM1. On the other hand, in the present study, we showed that the two mutations in ORAI1 directly caused constitutive opening of the channel, resulting in higher cytosolic Ca^{2+} influx independent of either Ca^{2+} stores in the SR or STIM1 activation.

ORAI1 is a tetra-spanning TM protein in the plasma membrane (Fig. 3C) (8), and acts as a pore subunit of the CRAC channel (29). The CRAC channel consists of a hexamer of ORAI1 proteins, and the TM helices (TM1 – 4) of each monomer are arranged in three concentric rings. Six TM1 helices make up an inner ring of helices and line the ion pore, while the TM2 and TM3 helices constitute a middle ring that surrounds the TM1 helices (24) (Fig. 3D). The mutation c.292G.A (Gly98Ser) was identified in the TM1 domain directly beside the pore (white residues in Fig. 3D). The other mutation, p.412C.T (Leu138Phe), was identified in the TM2 domain directly facing TM1 (yellow residues in Fig. 3D).

Many studies have elucidated the roles of amino acid residues in TM1 in channel activity as well as in the ion selectivity of SOCE channels (8,29 – 33). In particular, Arg91 is mutated in SCID (13) and is thought to act as both a barrier as well as a provider of electrostatic stabilization to the elongated pore that is controlled via interaction with STIM1, and Glu106 determines ion selectivity (8) (Fig. 3C). Similarly, the importance of Gly98 for channel activity has also been suggested based on in vitro experiments (31). Interestingly, Gly98 has been predicted to be located exactly two a-helical turns from both the Arg91 and Glu106 sites (Fig. 3C). Ala replacement at Gly98 results in failure of channel activity, whereas Asp or Pro replacement at this position results in a negative charge or hydrophilic properties, which in turn cause constitutive channel opening as well as reduced ion selectivity in a STIM1-independent manner (31,33). Our experiments revealed that a Ser replacement of Gly at position 98 may also confer the protein with a hydrophilic

Table 2. Histological characterization of TAM families

	Family A	Family B			Family C
	II-3	I-2	II-1	II-3	II-1
Age at muscle biopsy	42 years	NI	10 years	5 years	42 years
Tubular aggregates	Type I and II fibers	+	Type I and II fibers	2	Type I and II fibers
Fiber size variation	+	NI	+	+	+
Regenerating fibers	+	NI	+	2	+
Increased internal nuclei (% of fibers)	Single 14%	NI	Single 15%	Single 5%	Single, multiple 20%
Type I fiber predominance (% of fibers)	70%	NI	71%	93%	73%

NI, no information.

property that is sufficient to cause constitutive channel activation, similar to the effect of Pro replacement.

In contrast to TM1, the roles of specific amino acid residues in TM2 have not been well investigated. In our experiment, the mutation c.412C.T (p.Leu138Phe) in TM2 also caused constitutive SOCE channel activation. Interestingly, basal $[Ca^{2+}]_i$ levels in Leu138Phe-expressing HEK293 cells were lower than those were in Gly98Ser-expressing cells. Further studies are necessary to fully understand the impact of these mutations on CRAC channels.

Of particular note, the mechanism underlying the muscle weakness caused by a constitutively activated CRAC channel might be associated with altered Ca^{2+} homeostasis in a manner different from that derived from its loss of function. Individuals affected with SCID owing to recessive loss-of-function mutations in ORAI1 or STIM1 were reported to show muscle hypotonia (13 – 15) and decreased Ca^{2+} influx. Transgenic mice with muscle-specific expression of dominant-negative Orai1 have also been reported and exhibited reduced body weight, muscle mass and fiber cross-sectional area, and increased susceptibility to fatigue, which might have been due to SR Ca^{2+} depletion (34). On the other hand, ORAI1-related TAM is caused by elevation of $[Ca^{2+}]_i$ levels in the skeletal muscle cells, similar to STIM1-related TAM. Therefore, preventing excessive extracellular Ca^{2+} influx is a potential therapeutic strategy for TAM.

The mechanism of TA formation in the skeletal muscle has remained elusive thus far. However, our results support the hypothesis that TA formation is related to disordered Ca^{2+} homeostasis. Recent efforts on the identification of causative genes in TA-presenting muscle diseases also provide a clue into this mechanism. Recessive mutations in GFPT1 and DPAGT1, which are both involved in protein N-glycosylation, have been shown to be causative factors of myasthenic syndrome with TAs (35,36). Furthermore, the functional importance of N-glycosyl modification of STIM1 was recently reported (27). A mutation at the N-glycosylation site in STIM1 results in a strong gain of function by increasing the number of active Orai1 channels, indicating the significance of N-glycosylation for the function of STIM. Thus, activation of CRAC channels may result in the formation of TAs in skeletal muscles, although further analyses of CRAC channel activation in skeletal muscles of GFPT1- and DPAGT1-mutated individuals are required to confirm this hypothesis.

The finding of c.292G.A (p.Gly98Ser) ORAI1 mutation in two unrelated families would not be due to a founder effect. This mutation in Family A probably occurred de novo in II-3a because individual I-1a did not show any symptoms of myopathy in his lifetime and individual I-2a does not have the mutation. Regarding to the mutation in Family B, we could not judge whether it is de novo or not, because of limited information.

The clinical and histological features of ORAI1-mutated TAM are similar to those of TAM caused by STIM1 mutations, regarding onset of the disease, progression of weakness, involvement of contractures, presence of TAs in both type I and type II fibers, fiber size variation and type I fiber predominance. However, the patterns of affected muscles are slightly different: individuals with ORAI1-mutated TAM exhibit diffuse weakness in all limbs, and the characteristic patterns in the selectivity of atrophy, whereas those with STIM1-mutated TAM show proximal muscle weakness only in the lower limbs (16). Severe ankle contractures and a rigid spine were common characteristics observed in the families included in the present study, although STIM1-mutated TAM was not likely. Furthermore, eye-movement defects, which were reported in STIM1-mutated TAM individuals studied by Böhm et al. (16), congenital miosis, bleeding diathesis and thrombocytopenia are not detected in individuals with ORAI1-mutated TAM. This discrepancy could be explained by differences in the expression patterns of STIM1, ORAI1 and their homologues (ORAI2, ORAI3 and STIM2).

Although ORAI1 transcripts are expressed in multiple tissues, including the skeletal muscle, in humans and mice (28,37), it is not clear why other organs were saved. Orai1 expression is low in the brain (28); therefore, the intellectual disability observed in individual III-2a in the present study might be unrelated to the ORAI1 mutation. The calcification in the brain of individual II-3a could be attributed to long-term hypocalcemia.

Another characteristic clinical feature of ORAI1-mutated TAM is hypocalcemia. Serum Ca^{2+} levels are controlled mainly through the action of PTH and 1,25(OH)2D3 (38). These hormones increase the serum Ca^{2+} level through their actions on the bone, kidney and intestine; impaired activity of either hormone leads to hypocalcemia. In this study, the five individuals analyzed showed mildly decreased serum Ca^{2+} levels and rather low PTH levels, which were nonetheless within the normal range. PTH is secreted by parathyroid cells and the secretion volume is controlled by the extracellular Ca^{2+} intensity. In ORAI1-mutated TAM individuals, PTH levels are improperly low in spite of the presence of hypocalcemia. This condition is classified as PTH-insufficient hypoparathyroidism on the basis of the criteria for the differential diagnosis of hypocalcemia

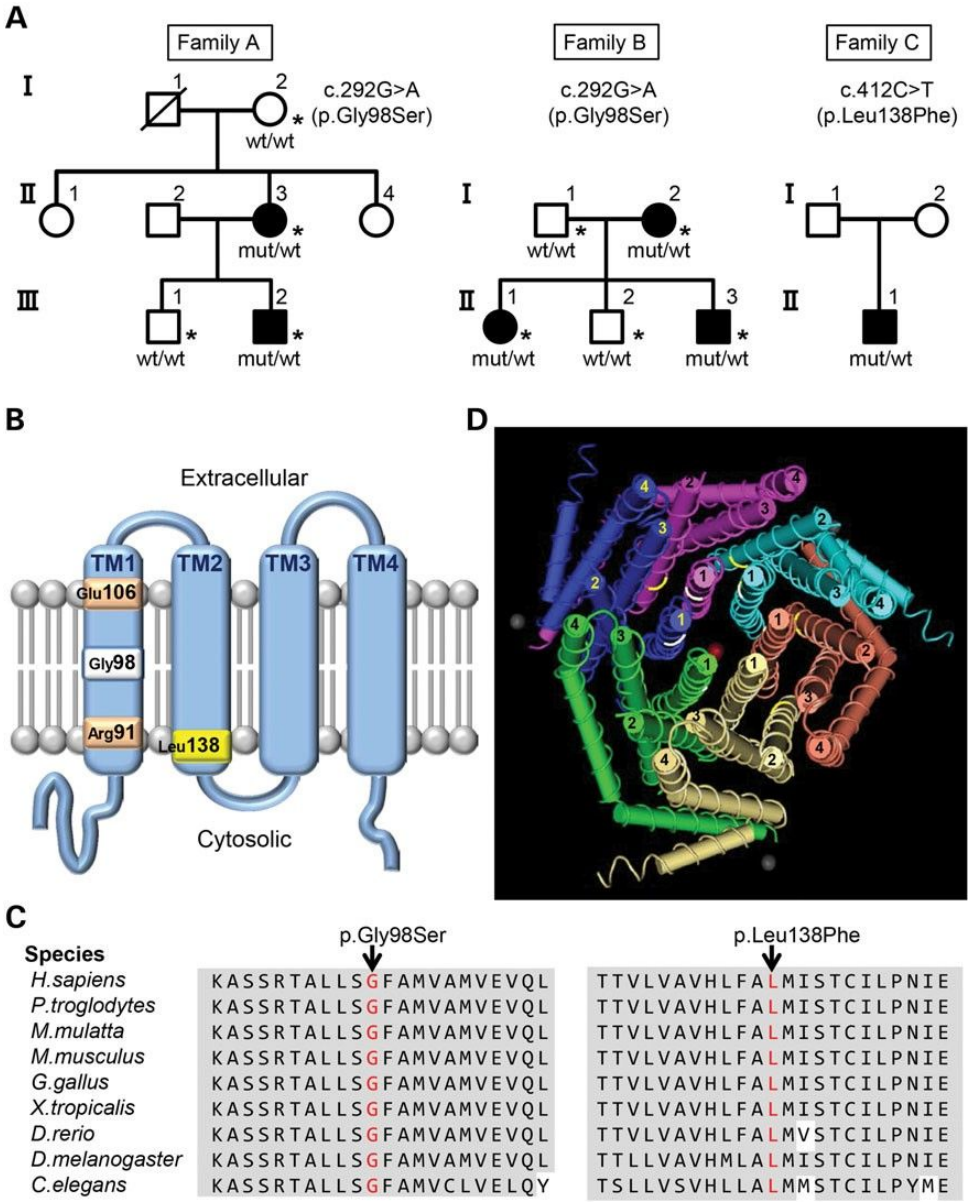

Figure 3. Genetic analysis of autosomal-dominant TAM and modeling the effects of mutations in ORAI1. (A) Pedigrees indicated dominant inheritance of TAM, and sequence analysis confirmed the segregation of the heterozygous mutations with the disease. * Individuals who were analyzed by exome sequencing. ORAI1 genotypes are shown below the individuals in the pedigrees. (B) Schematic depiction of a single ORAI1 subunit. Upper side, extracellular; lower side, cytosolic. Gly98Ser and Leu138Phe are highlighted in white and yellow, respectively. Arg91 and Glu106, critical amino acids for channel function, are shown in orange. (C) Amino acid sequence conservation of ORAI1. The affected amino acids (red) have been highly conserved during evolution. (D) Crystal structure of the Drosophila melanogaster SOCE channel. The crystal structure was obtained from the Molecular Modeling Database (MMDB ID: 105660). This structure shows that the channel is formed from a hexamer of ORAI subunits. Each subunit is represented in a different color. The ion pore is located at the center of the channel (red circle), and the transmembrane helices are arranged in three concentric rings. Six TM1 helices (1) make up an inner ring of helices and line the ion pore. The TM2 (2) and TM3 (3) helices constitute a middle ring that surrounds the transmembrane portion of the TM1 helices and separates them from TM4 helices (4), which are arranged in an outer ring. The position of Gly98 in TM1 is highlighted in white, and that of Leu138 in TM2 is highlighted in yellow.

(39). Although the precise pathomechanisms are not known, ORAI1-mutated TAM might cause decreased PTH secretion.

In summary, we identified heterozygous missense mutations in ORAI1 that cause TAM with hypocalcemia via constitutive activation of CRAC channels. Our results, together with those of previous reports (16,19), will contribute to establishing a new disease entity whose pathomechanism is associated with intracellular Ca^{2+} elevation to induce muscle weakness and TA formation in the skeletal muscles. The detailed pathomechanism linking intracellular Ca^{2+} elevation to muscle weakness and TA formation in the skeletal muscles should be clarified.

MATERIALS AND METHODS

Materials

Three unrelated Japanese families affected by TAM were selected based on pathological examinations. All clinical

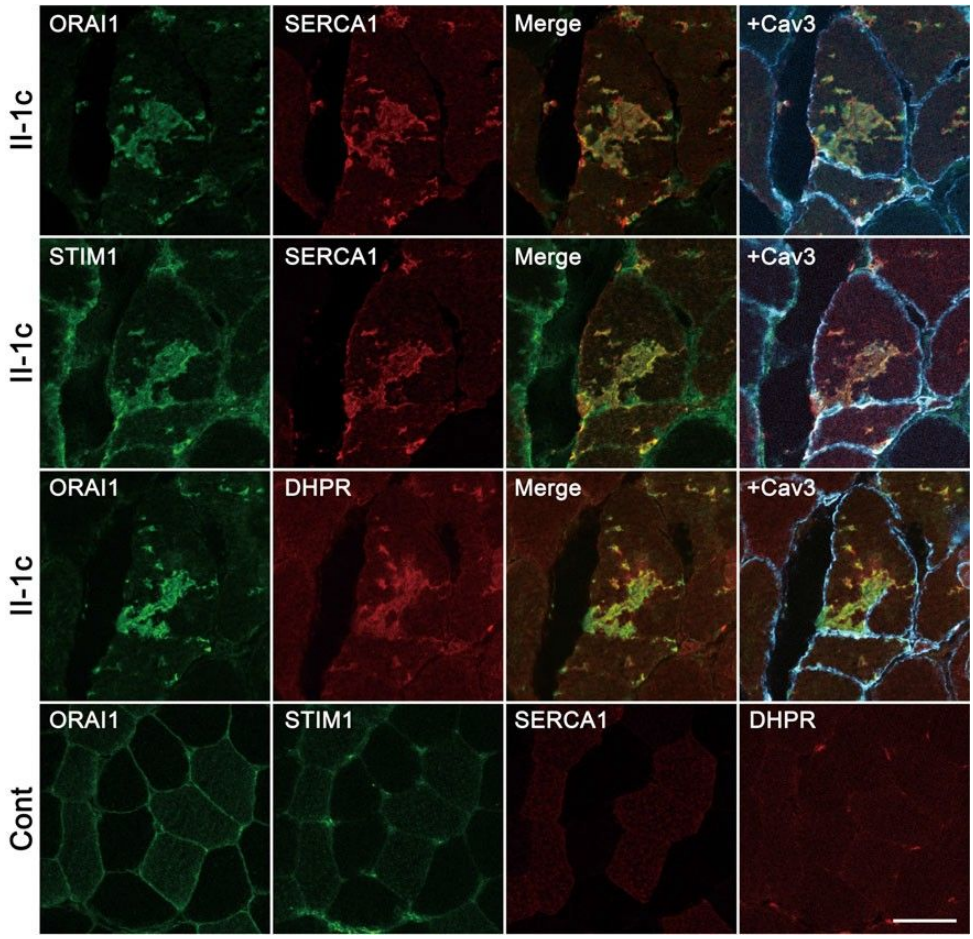

Figure 4. Immunohistochemical analysis of the skeletal muscle from an individual affected with TAM (II-1c). Immunofluorescence showed that SERCA1, ORAI1, STIM1 and DHPR localized in TAs. Scale bar, 50 mm. Cont, skeletal muscle from an unaffected person.

materials used in this study were obtained with written informed consent for research use. All experiments performed in this study were approved by the Ethical Committee of the National Center of Neurology and Psychiatry (NCNP).

Histological analyses

Muscle samples were taken from the biceps brachii. Muscles were frozen in liquid nitrogen-cooled isopentane and stored at 2808C. Serial frozen sections (10 mm thick) were histochemically stained with mGt, NADH-TR or SDH. Immunohistochemistry was performed using 8 mm thick serial frozen sections according to the standard protocols (40). The primary antibodies used were as follows: anti-Orai1 (O8264, 1:200 dilution; Sigma-Aldrich), anti-STIM1 (H-180, 1:50; Santa Cruz Biotechnology), anti-SERCA1 (VE121G9, 1:200; Abcam), anti-RYR1 (XA7B6, 1:200; Developmental Studies Hybridoma Bank) and anti-DHPR (IIID5E1, 1:100; Developmental Studies Hybridoma Bank). Anti-caveolin antibody (N-18, 1:100; Santa Cruz Biotechnology) was also used for labeling the sarcolemma (plasma membrane of the muscle fiber). After incubation with primary antibodies, the sections were incubated with appropriate Alexa Fluor 488-, 568- and 647-conjugated secondary antibodies (1:600; Invitrogen). The sections were observed under an LSM710 confocal laser microscope (Carl Zeiss).

Electron microscopy

Muscle specimens were fixed in 2.5% glutaraldehyde and post-fixed with 2% osmium tetroxide. Ultrathin sections of muscles stained with uranyl acetate and lead citrate were observed under a transmission electron microscope (FEI; Hillsboro, OR, USA).

Exome sequencing

Genomic DNA was isolated from muscle specimens or peripheral blood lymphocytes using standard techniques. Exome sequencing was carried out in subjects I-2a, II-3a, III-1a and III-2a from Family A, and in subjects I-1b, I-2b, II-1b, II-2b and II-3b from Family B. Exons of genomic DNA samples were captured and sequenced using Agilent in-solution enrichment methodology and the Illumina HiSeq1000 sequencer. Briefly, 3 mg of each genomic DNA sample was fragmented to 150 – 200 bp by sonication. Paired-end fragment libraries were prepared by using a kit from Agilent Technologies. Purified libraries (750 ng) were hybridized to the SureSelect oligonucleotide probe capture library for 24 h (Sure Select Human All Exon kit V4, 50 Mb; Agilent). The captured DNA sample was then sequenced on an Illumina HiSeq1000 as paired-end 100-base reads. Image analysis and base calling were performed using

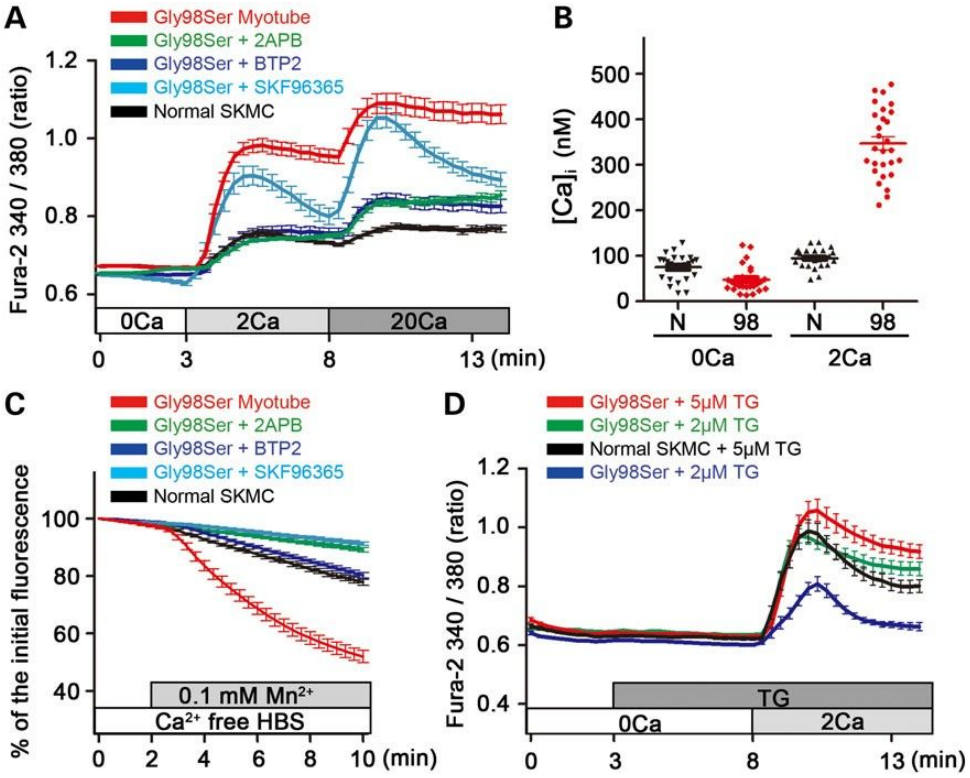

Figure 5. Cytosolic Ca^{2+} measurement and Mn^{2+} quenching assay of myotubes from an individual affected with TAM. (A) Cytosolic Ca^{2+} was measured with Fura-2 in myotubes from affected individual II-3b (red: Gly98Ser myotube, n ¼ 29 cells) and normal human skeletal muscle (black: normal SKMC, n ¼ 26 cells), using single-cell Ca^{2+} imaging. First, cells were placed in an extracellular solution containing 0 mM Ca^{2+} (0Ca). After 3 min, the extracellular solution was changed to 2 mM Ca^{2+} (2Ca), and then to 20 mM Ca^{2+} (20Ca) at 8 min. Myotubes from affected individual were experimentally treated with 50 mM 2-APB (green: Gly98Ser +2APB, n ¼ 17 cells), with 10 mM BTP-2 (blue: Gly98Ser +BTP2, n ¼ 17 cells) or with 20 mM SKF96365 (cyan: Gly98Ser +SKF96365, n ¼ 15). (B) Resting $[Ca^{2+}]_i$ in myotubes from TAM. 0Ca, N: normal SKMC98, n ¼ 26; 0Ca, 98: Gly98Ser myotube, n ¼ 25; 2Ca, N: normal SKMC98, n ¼ 27; 2Ca, 98: Gly98Ser myotube, n ¼ 28. (C) Fluorescence quenching due to the Mn^{2+} influx was observed in Fura-2-loaded Gly98Ser myotubes (red, n ¼ 32 cells) and normal SKMC myotubes (black, n ¼ 21 cells), using single-cell Ca^{2+} imaging. Mn^{2+} (0.1 mM) was added to nominally Ca^{2+}-free HBS. Gly98Ser myotubes were treated with 50 mM 2-APB (green: Gly98Ser + 2APB, n ¼ 17 cells), with 10 mM BTP-2 (blue: Gly98Ser + BTP2, n ¼ 17 cells) or with 20 mM SKF96365 (cyan: Gly98Ser +SKF96365, n ¼ 39 cells). (D) Store-operated Ca^{2+} entry in myotubes. Ca^{2+} stores in the SR were depleted by treatment with 2 mM TG or 5 mM TG. Red, Gly98Ser myotubes with 5 mM TG, n ¼ 20 cells; green, Gly98Ser myotubes with 2 mM TG, n ¼ 25 cells; black, normal SKMC myotubes with 5 mM TG, n ¼ 27 cells; blue, normal SKMC myotubes with 2 mM TG, n ¼ 25 cells.

the Illumina Real-Time Analysis Pipeline version 1.13, with default parameters.

Bioinformatics analysis

Reads were aligned to hg19 with Burrows-Wheeler Aligner (41). Duplicate reads were removed using Picard for downstream analysis. Local realignments around indels and regions for low base quality scores were performed with the Genome Analysis Toolkit (42) (GATK) for recalibration. Single-nucleotide variants and small indels were identified using GATK UnifiedGenotyper (version 1.6) and filtered according to the Broad Institute's best-practice guidelines. Genetic variation was annotated with the NCNP in-house pipeline (amelief), consisting of gene annotation [using ANNOVAR (43)] and detection of known polymorphisms using dbSNP135, the 1000 Genomes, NHLBI Exome Variant Server (ESP5400) and HGVD for Japanese genetic variants. Candidates of mutations identified in exome sequencing were validated by Sanger sequencing on an ABI Prism 3130 DNA Analyzer (Applied Biosystems). Segregation analysis of within-family variants was carried out using the primer sets designed to amplify exons corresponding to the sequence under accession NM_032790. PCR conditions and primer sequences for ORAI1 mutation analysis are available upon request.

Western blotting of the skeletal muscles

Frozen skeletal muscles were sliced and suspended in the buffer containing 10 mM Tris – HCl, 0.6 mM KCl and 1 mM EDTA. After a centrifugation at 1200g for 10 min, the supernant was centrifuged at 20 000g for 90 min. The resulting pellet was solubilized in laemmli's sample buffer. An equal amount of proteins (10 mg) were electrophoresed on 4 – 20% polyacrylamide gradient gel (Bio-Rad). The primary antibodies used were as follows: anti-Orai1 (O8264, 1:1000 dilution; Sigma-Aldrich), anti-STIM1 (H-180, 1:500; Santa Cruz Biotechnology), anti-SERCA1 (VE121G9, 1:1000; Abcam) and anti-caveolin-3 antibody (Clone 26, 1:1000; BD Transduction Laboratories). The blots were coupled with the peroxidase-conjugated secondary antibodies, and developed using the ECL detection kit (Millipore Corporation).

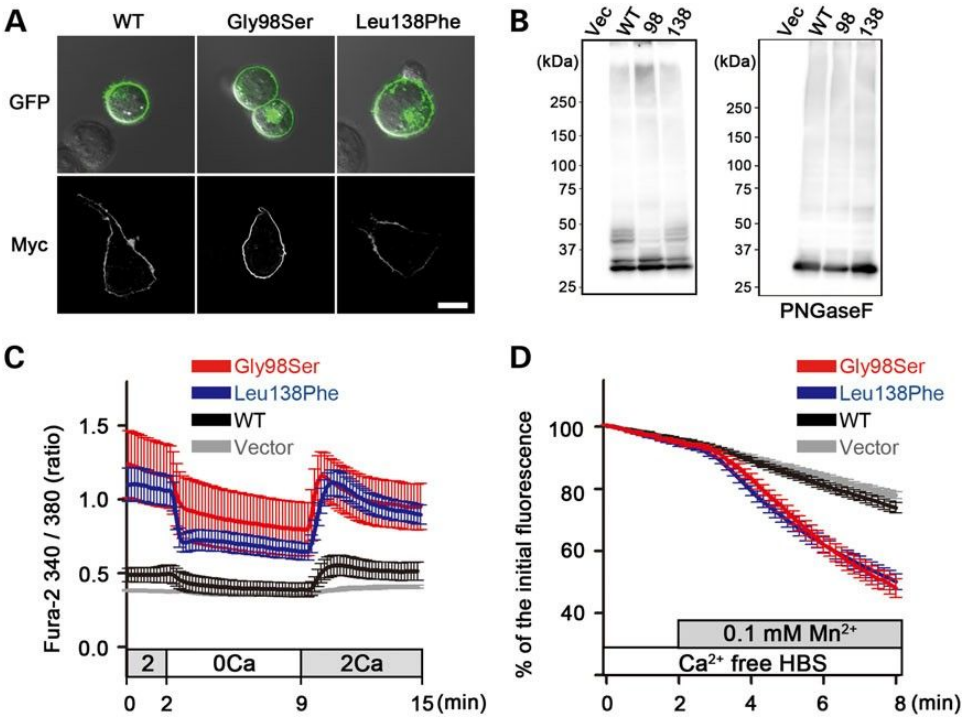

Figure 6. Characterization of ORAI1 mutants. (A) Localization of transfected ORAI1 constructs. HEK 293 cells were transfected with EGFP-tagged ORAI1 (WT, Gly98Ser, Leu138Phe) or Myc-tagged ORAI1 (WT, Gly98Ser, Leu138Phe). Upper panels, phase contrast (white and black) and GFP fluorescence (green). Lower panels, fluorescent micrographs for Myc-ORAI1. (B) Western blot of Myc-tagged ORAI1 proteins expressed in HEK cells (left panel). PGNaseF treatment (right panel). Vec, vector; 98, ORAI1 with Gly98Ser; 138, ORAI1 with Leu138Phe. (C) Cytosolic Ca^{2+} was measured in HEK293 cells expressing WT ORAI1 (black, n ¼ 35 cells) and ORAI1 mutants, Gly98Ser (red, n ¼ 28 cells) or Leu138Phe (blue, n ¼ 37 cells) and vector (gray, n ¼ 32 cells). Extracellular solution was first changed to 0 mM Ca^{2+} (0Ca) then to 2 mM Ca^{2+} (2Ca). (D) Mn^{2+} quenching assay. After application of 0.1 mM Mn^{2+} solution, fluorescence quenching of Fura-2 was observed in HEK293 cells expressing WT ORAI1 (black, n ¼ 34 cells) and ORAI1 mutants, G98S (red, n ¼ 42 cells) or L138F (blue, n ¼ 43 cells), and vector (gray, n ¼ 46 cells).

Construction of ORAI1 mutants

The construction of WT and mutant human ORAI1 cDNA in the expression vectors pCMV-Myc and pEGFP-N1 (Clontech) was described previously (44). A Myc tag was fused to the N-terminus of ORAI1, and a EGFP tag was fused to the C-terminus of ORAI1 without its termination codon. All ORAI1 mutants were generated with the Quick Change Site-Directed Mutagenesis Kit (Stratagene). Information on primer sequences and conditions for cloning and PCR is available upon request.

Transfection of ORAI1 constructs to HEK293 cells

HEK293 cells obtained from the RIKEN Bioresource Center were maintained in Dulbecco's modified Eagle medium (D-MEM; Wako) supplemented with 10% fetal bovine serum (FBS; Life Technologies), 2 mM glutamine, 30 units/ml penicillin and 30 mg/ml streptomycin. ORAI1 constructs were transfected using X-tremeGENE9 (Roche Applied Science). For observation of ORAI1 mutants in cells, EGFP-tagged ORAI1 constructs were also introduces. For western blots, Myc-tagged ORAI1 constructs were introduced. For $[Ca^{2+}]_i$ measurement, Myc-tagged ORAI1 constructs were co-transfected with the pDsRed-Monomer-C1 vector (Clontech).

Localization of ORAI1 protein in HEK293 cells

Confocal and phase contrast images were taken at 2 days post-transfection on an LSM-710 microscope (Carl Zeiss).

Expression of ORAI1 protein in HEK293 cells

HEK293 cells were harvested at 2 days post-transfection. The cells were lysed with Tris-buffered saline containing 1% Triton X-100 and protease inhibitors (cOmplete EDTA-free; Roche). The extracts were boiled in the presence of sodium dodecyl sulfate sample buffer and subjected to western blot analysis. An equal amount of the supernatant fractions (75 mg proteins) was subjected to SDS–PAGE (SuperSep Ace, 5–20% gradient gel, Wako). The protein-transferred membrane was incubated with anti-Myc antibody (9E10, 1:2000; Wako). After incubating with anti-mouse IgG (H+L) secondary antibody conjugated with horseradish peroxidase (GE Healthcare), the expression of ORAI1-Myc was detected using Immunostar Zeta (Wako). To confirm glycosylated patterns of ORAI1, lysate samples (75 mg each) were incubated with PNGase F (Roche; 3 U/sample), for 6 h at 378C and subjected to SDS–PAGE.

Cell culture for $[Ca^{21}]_i$ measurement and Mn^{21} quenching assay

Skeletal muscle cells of a TAM-affected individual (II-3b) and normal human SKMCs (Clonetics) were seeded onto collagen-coated glass cover slips and cultured in D-MEM/Ham's F-12 medium (1:1) supplemented with 20% FBS (Invitrogen), 100 units/ml penicillin and 100 mg/ml streptomycin. After the cells reached confluence, the culture media were switched to differentiation media [D-MEM/Ham's F-12 Medium (1:1)

supplemented with 5% horse serum (Invitrogen), 100 units/ml penicillin and 100 mg/ml streptomycin]. Six days following induction of differentiation, myotubes were used for $[Ca^{2+}]_i$ imaging or a Mn^{2+} quenching assay.

Transfected HEK293 cells were lifted using trypsin and seeded onto poly-L-lysine-coated glass cover slips at 8 h post-transfection. Note that trypsinized cells were cultured in low-Ca^{2+} D-MEM (Life Technologies), which was supplemented with 10% FBS, 2 mM glutamine, 30 units/ml penicillin, 30 mg/ml streptomycin, 0.2 mM $CaCl_2$ and 10 mM La^{3+}, to prevent Ca^{2+} overload-induced cell death (31). $[Ca^{2+}]_i$ imaging was performed at 24–36 h after transfection.

Measurement of changes in $[Ca^{21}]_i$

HEK293 cells on cover slips were loaded with Fura-2 by incubation in low-Ca^{2+} D-MEM containing 5 mM Fura-2/AM (Dojindo Laboratories) at 378C for 40 min, and washed with imaging solution (2Ca). The cover slips were then placed in a perfusion chamber mounted on the stage of a microscope (Axio-observer Z1; Carl Zeiss). Transfected cells were identified by detection of fluorescence from pDsRed-Monomer. Fura-2 fluorescence images of the cells were recorded and analyzed with Physiology software (Carl Zeiss). The 340/380 nm ratios of images were recorded at 10 s intervals. The compositions of $[Ca^{2+}]_i$ imaging solutions are listed in Supplementary Material, Table S6. Fura-2/AM was loaded into skeletal myotubes on cover slips in the same manner used for HEK293 cells but in nominally Ca^{2+}-free HEPES-buffered saline (HBS) (Supplementary Material, Table S6). The cover slips were then placed in a perfusion chamber mounted on the stage of the microscope (IX70; Olympus). Fura-2 fluorescence images of the myotubes were recorded and analyzed with MetaMorph Imaging Software (Molecular Devices). The images were recorded at 20 s intervals. Compositions of $[Ca^{2+}]_i$ imaging solutions are listed in Supplementary Material, Table S6. For measurement of the resting $[Ca^{2+}]_i$, Fura-2/AM was loaded to myotubes at 0Ca and 2Ca, respectively, and $[Ca^{2+}]_i$ imaging was performed. The resting $[Ca^{2+}]_i$ was calculated as previously reported (45).

Mn^{21} quenching assay

Extracellular Mn^{2+} entry was measured through monitoring the decline in the fluorescence intensity of Fura-2 at an isosbestic excitation wavelength of 360 nm and recording the emitted fluorescence at 510 nm (46) by using the same system as used for the $[Ca^{2+}]_i$ measurement. The compositions of nominally Ca^{2+}-free HBS and 0.1 mM $MnCl_2$ solutions are listed in Supplementary Material, Table S6.

Statistical analysis

Graphics were prepared and statistical analyses were performed with GraphPad Prism (GraphPad Software). Data are presented as mean + SEM. All data were analyzed using unpaired t-tests in comparisons between two samples and ANOVA in comparisons among three samples.

WEB RESOURCES

Online Mendelian Inheritance in Man (OMIM), http://www.omim.org/.
dbSNP, http://www.ncbi.nlm.nih.gov/projects/SNP/.
1000 Genomes Project, http://www.1000genomes.org/.
NHLBI Exome Sequencing Project (ESP) Exome Variant Server, http://eversusgs.washington.edu/EVS/.
HGVD, http://www.genome.med.kyoto-u.ac.jp/SnpDB/.
MutationTaster, http://www.mutationtaster.org/.
SIFT, http://sift.jcvi.org.
PolyPhen-2, http://genetics.bwh.harvard.edu/pph2/.
MMDB, http://www.ncbi.nlm.nih.gov/Structure/MMDB/mmdb.shtml.
BWA, http://bio-bwa.sourceforge.net/.
Picard, http://picard.sourceforge.net/.
GATK, http://www.broadinstitute.org/gatk/.
ANNOVAR, http://www.openbioinformatics.org/annovar/.

SUPPLEMENTARY MATERIAL

Supplementary Material is available at HMG online.

ACKNOWLEDGEMENTS

We thank T. Uchiumi, K. Goto, A. Kaminaga, K. Tatezawa and M. Ogawa for technical assistance. The antibodies XA7B6 for anti-RYR1 and IIID5E1 for anti-DHPR developed by K.P. Campbell were obtained from the Developmental Studies Hybridoma Bank developed under auspices of the NICHD and maintained by the University of Iowa, Department of Biology, Iowa City, IA52242.

Conflict of Interest statement. None declared.

FUNDING

This work was supported by an Intramural Research Grant (26-8, 25-5, 23-4) for Neurological and Psychiatric Disorders of the NCNP (to S.N., Y.H., I.N.) and by a Research on Applying Health Technology grant (H23-JITSUYOUKA(NANBYOU)-IPPAN-008, H26-ITAKU(NAN)-IPPAN-081) from the Ministry of Health, Labour and Welfare (to I.N.).

REFERENCES

1. Shoback, D. (2008) Clinical practice. Hypoparathyroidism. New Eng. J. Med., 359, 391–403.
2. Rossi, A.E. and Dirksen, R.T. (2006) Sarcoplasmic reticulum: the dynamic calcium governor of muscle. Muscle Nerve, 33, 715–731.
3. Vig, M., Peinelt, C., Beck, A., Koomoa, D.L., Rabah, D., Koblan-Huberson, M., Kraft, S., Turner, H., Fleig, A., Penner, R. and Kinet, J.P. (2006) CRACM1 is a plasma membrane protein essential for store-operated Ca^{2+} entry. Science, 312, 1220–1223.
4. Yeromin, A.V., Zhang, S.L., Jiang, W., Yu, Y., Safrina, O. and Cahalan, M.D. (2006) Molecular identification of the CRAC channel by altered ion selectivity in a mutant of Orai. Nature, 443, 226–229.
5. Liou, J., Kim, M.L., Heo, W.D., Jones, J.T., Myers, J.W., Ferrell, J.E. and Meyer, T. (2005) STIM is a Ca^{2+} sensor essential for Ca^{2+}-store-depletion-triggered Ca^{2+} influx. Curr. Biol., 15, 1235–1241.
6. Roos, J., DiGregorio, P.J., Yeromin, A.V., Ohlsen, K., Lioudyno, M., Zhang, S., Safrina, O., Kozak, J.A., Wagner, S.L., Cahalan, M.D. et al. (2005) STIM1, an essential and conserved component of store-operated Ca^{2+} channel function. J. Cell Biol., 169, 435–445.
7. Zhang, S.L., Yu, Y., Roos, J., Kozak, J.A., Deerinck, T.J., Ellisman, M.H., Stauderman, K.A. and Cahalan, M.D. (2005) STIM1 is a Ca^{2+} sensor that

activates CRAC channels and migrates from the Ca^{2+} store to the plasma membrane. Nature, 437, 902–905.
8. Prakriya, M., Feske, S., Gwack, Y., Srikanth, S., Rao, A. and Hogan, P.G. (2006) Orai1 is an essential pore subunit of the CRAC channel. Nature, 443, 230–233.
9. Stathopulos, P.B., Li, G.-Y., Plevin, M.J., Ames, J.B. and Ikura, M. (2006) Stored Ca^{2+} depletion-induced oligomerization of stromal interaction molecule 1 (STIM1) via the EF-SAM region: an initiation mechanism for capacitive Ca^{2+} entry. J. Biol. Chem., 281, 35855–35862.
10. Luik, R.M., Wu, M.M., Buchanan, J. and Lewis, R.S. (2006) The elementary unit of store-operated Ca^{2+} entry: local activation of CRAC channels by STIM1 at ER-plasma membrane junctions. J. Cell Biol., 174, 815–825.
11. Park, C.Y., Hoover, P.J., Mullins, F.M., Bachhawat, P., Covington, E.D., Raunser, S., Walz, T., Garcia, K.C., Dolmetsch, R.E. and Lewis, R.S. (2009) STIM1 clusters and activates CRAC channels via direct binding of a cytosolic domain to Orai1. Cell, 13, 876–890.
12. Wu, M.M., Buchanan, J., Luik, R.M. and Lewis, R.S. (2006) Ca^{2+} store depletion causes STIM1 to accumulate in ER regions closely associated with the plasma membrane. J. Cell Biol., 174, 803–813.
13. Feske, S., Gwack, Y., Prakriya, M., Srikanth, S., Puppel, S.-H., Tanasa, B., Hogan, P.G., Lewis, R.S., Daly, M. and Rao, A. (2006) A mutation in Orai1 causes immune deficiency by abrogating CRAC channel function. Nature, 441, 179–185.
14. McCarl, C.A., Picard, C., Khalil, S., Kawasaki, T., Röther, J., Papolos, A., Kutok, J., Hivroz, C., Ledeist, F., Plogmann, K., Ehl, S. et al. (2009) ORAI1 deficiency and lack of store-operated Ca^{2+} entry cause immunodeficiency, myopathy, and ectodermal dysplasia. J. Allergy Clin. Immunol., 124, 1311–1318.
15. Picard, C., McCarl, C.-A., Papolos, A., Khalil, S., Lüthy, K., Hivroz, C., LeDeist, F., Rieux-Laucat, F., Rechavi, G., Rao, A. et al. (2009) STIM1 mutation associated with a syndrome of immunodeficiency and autoimmunity. New Eng. J. Med., 360, 1971–1980.
16. Böhm, J., Chevessier, F., Maues De Paula, A., Koch, C., Attarian, S., Feger, C., Hantaï, D., Laforêt, P., Ghorab, K., Vallat, J.M. et al. (2013) Constitutive activation of the calcium sensor STIM1 causes tubular-aggregate myopathy. Am. J. Hum. Genet., 92, 271–278.
17. Jain, D., Sharma, M.C., Sarkar, C., Suri, V., Sharma, S.K., Singh, S. and Das, T.K. (2008) Tubular aggregate myopathy: a rare form of myopathy. J. Clin. Neurosci., 15, 1222–1226.
18. Nesin, V., Wiley, G., Kousi, M., Ong, E.C., Lehmann, T., Nicholl, D.J., Suri, M., Shahrizaila, N., Katsanis, N., Gaffney, P.M., Wierenga, K.J. and Tsiokas, L. (2014) Activating mutations in STIM1 and ORAI1 cause overlapping syndromes of tubular myopathy and congenital miosis. Proc. Natl Acad. Sci. USA, 11, 4197–4202.
19. Misceo, D., Holmgren, A., Louch, W.E., Holme, P.A., Mizobuchi, M., Morales, R.J., De Paula, A.M., Stray-Pedersen, A., Lyle, R., Dalhus, B. et al. (2014) A dominant STIM1 mutation causes Stormorken syndrome. Hum. Mutat., 35, 556–564.
20. Chevessier, F., Marty, I., Paturneau-Jouas, M., Hantaï, D. and Verdière-Sahuqué, M. (2004) Tubular aggregates are from whole sarcoplasmic reticulum origin: alterations in calcium binding protein expression in mouse skeletal muscle during aging. Neuromus. Disord., 14, 208–216.
21. Chevessier, F., Bauché-Godard, S., Leroy, J.-P., Koenig, J., Paturneau-Jouas, M., Eymard, B., Hantaï, D. and Verdière-Sahuqué, M. (2005) The origin of tubular aggregates in human myopathies. J. Pathol., 207, 313–323.
22. Salviati, G., Pierobon-Bormioli, S., Betto, R., Damiani, E., Angelini, C., Ringel, S.P., Salvatori, S. and Margreth, A. (1985) Tubular aggregates: sarcoplasmic reticulum origin, calcium storage ability, and functional implications. Muscle Nerve, 8, 299–306.
23. Schiaffino, S. (2012) Tubular aggregates in skeletal muscle: just a special type of protein aggregates? Neuromuscul. Disord., 22, 199–207.
24. Hou, X., Pedi, L., Diver, M.M. and Long, S.B. (2012) Crystal structure of the calcium release-activated calcium channel Orai. Science, 338, 1308–1313.
25. Prakriya, M. and Lewis, R.S. (2001) Potentiation and inhibition of Ca^{2+} release-activated Ca^{2+} channels by 2-aminoethyldiphenyl borate (2-APB) occurs independently of IP(3) receptors. J. Physiol., 536, 3–19.
26. Ishikawa, J., Ohga, K., Yoshino, T., Takezawa, R., Ichikawa, A., Kubota, H. and Yamada, T. (2003) A pyrazole derivative, YM-58483, potently inhibits store-operated sustained Ca^{2+} influx and IL-2 production in T lymphocytes. J. Immunol., 170, 4441–4449.
27. Kilch, T., Alansary, D., Peglow, M., Dörr, K., Rychkov, G., Rieger, H., Peinelt, C. and Niemeyer, B.A. (2013) Mutations of the Ca^{2+}-sensing stromal interaction molecule STIM1 regulate Ca^{2+} influx by altered oligomerization of STIM1 and by destabilization of the Ca^{2+} channel Orai1. J. Biol. Chem., 288, 1653–1664.
28. Gwack, Y., Srikanth, S., Feske, S., Cruz-Guilloty, F., Oh-hora, M., Neems, D.S., Hogan, P.G. and Rao, A. (2007) Biochemical and functional characterization of Orai proteins. J. Biol. Chem., 282, 16232–16243.
29. Zhou, Y., Ramachandran, S., Oh-Hora, M., Rao, A. and Hogan, P.G. (2010) Pore architecture of the ORAI1 store-operated calcium channel. Proc. Natl Acad. Sci. USA, 107, 4896–4901.
30. Muik, M., Frischauf, I., Derler, I., Fahrner, M., Bergsmann, J., Eder, P., Schindl, R., Hesch, C., Polzinger, B., Fritsch, R. et al. (2008) Dynamic coupling of the putative coiled-coil domain of ORAI1 with STIM1 mediates ORAI1 channel activation. J. Biol. Chem., 283, 8014–8022.
31. Zhang, S.L., Yeromin, A.V., Hu, J., Amcheslavsky, A., Zheng, H. and Cahalan, M.D. (2011) Mutations in Orai1 transmembrane segment 1 cause STIM1-independent activation of Orai1 channels at glycine 98 and channel closure at arginine 91. Proc. Natl Acad. Sci. USA, 108, 17838–17843.
32. McNally, B.A., Somasundaram, A., Yamashita, M. and Prakriya, M. (2012) Gated regulation of CRAC channel ion selectivity by STIM1. Nature, 482, 241–245.
33. Zheng, H., Zhou, M.-H., Hu, C., Kuo, E., Peng, X., Hu, J., Kuo, L. and Zhang, S.L. (2013) Differential roles of the C and N termini of Orai1 protein in interacting with stromal interaction molecule 1 (STIM1) for Ca^{2+} release-activated Ca^{2+} (CRAC) channel activation. J. Biol. Chem., 288, 11263–11272.
34. Wei-Lapierre, L., Carrell, E.M., Boncompagni, S., Protasi, F. and Dirksen, R.T. (2013) Orai1-dependent calcium entry promotes skeletal muscle growth and limits fatigue. Nat. Commun., 4, 2805.
35. Senderek, J., Müller, J.S., Dusl, M., Strom, T.M., Guergueltcheva, V., Diepolder, I., Laval, S.H., Maxwell, S., Cossins, J., Krause, S. et al. (2011) Hexosamine biosynthetic pathway mutations cause neuromuscular transmission defect. Am. J. Hum. Genet., 88, 162–172.
36. Belaya, K., Finlayson, S., Slater, C.R., Cossins, J., Liu, W.W., Maxwell, S., McGowan, S.J., Maslau, S., Twigg, S.R., Walls, T.J. et al. (2012) Mutations in DPAGT1 cause a limb-girdle congenital myasthenic syndrome with tubular aggregates. Am. J. Hum. Genet., 91, 193–201.
37. Kiviluoto, S., Decuypere, J.P., De Smedt, H., Missiaen, L., Parys, J.B. and Bultynck, G. (2011) STIM1 as a key regulator for Ca^{2+} homeostasis in skeletal-muscle development and function. Skelet. Muscle, 1, 16.
38. Kumar, R. and Thompson, J.R. (2011) The regulation of parathyroid hormone secretion and synthesis. J. Am. Soc. Nephrol., 22, 216–224.
39. Fukumoto, S., Namba, N., Ozono, K., Yamauchi, M., Sugimoto, T., Michigami, T., Tanaka, H., Inoue, D., Minagawa, M., Endo, I. and Matsumoto, T. (2008) Causes and differential diagnosis of hypocalcemia—recommendation proposed by expert panel supported by ministry of health, labour and welfare, Japan. Endocr. J., 55, 787–794.
40. Malicdan, M.C., Noguchi, S. and Nishino, I. (2009) Monitoring autophagy in muscle diseases. Methods Enzymol., 453, 379–396.
41. Li, H. and Durbin, R. (2009) Fast and accurate short read alignment with Burrows-Wheeler transform. Bioinformatics, 25, 1754–1760.
42. DePristo, M.A., Banks, E., Poplin, R., Garimella, K.V., Maguire, J.R., Hartl, C., Philippakis, A.A., Angel, G., Rivas, M.A., Hanna, M. et al. (2009) A framework for variation discovery and genotyping using next-generation DNA sequencing data. Nat. Genet., 43, 491–498.
43. Wang, K., Li, M. and Hakonarson, H. (2010) ANNOVAR: functional annotation of genetic variants from high-throughput sequencing data. Nucleic Acids Res., 38, e164.
44. Maniatis, T., Fritsch, E.F. and Sambrook, J. (1982) Molecular Cloning: A Laboratory Manual. Cold Spring Harbor Laboratory Press, Cold Spring Harbor, NY.
45. Ihara, Y., Urata, Y., Goto, S. and Kondo, T. (2006) Role of calreticulin in the sensitivity of myocardiac H9c2 cells to oxidative stress caused by hydrogen peroxide. Am. J. Physiol. Cell Physiol., 290, C208–C221.
46. Pan, Z., Zhao, X. and Brotto, M. (2012) Fluorescence-based measurement of store-operated calcium entry in live cells: from cultured cancer cell to skeletal muscle fiber. J. Vis. Exp., 13, e3415.